X-Ray Diffraction and IR Spectrum for Activated Surface Hydrolysis of Al Metal into AlO(OH)·αH$_2$O Nanocrystals in a New Monoclinic Crystal Structure

S. Rana and S. Ram[1]

Materials Science Centre, Indian Institute of Technology, Kharagpur-721 302, India

Activated spontaneous surface hydrolysis of nascent Al metal in distilled water at room temperature results in AlO(OH)·αH$_2$O (boehmite) nanocrystals of an average 35 nm diameter. The nanocrystals are separated by 2 to 5 nm with a fairly sharp size distribution in the electron micrograph. Their X-ray diffraction is analyzed by assuming a monoclinic crystal structure with lattice parameters $a = 0.866$ nm, $b = 0.506$ nm, $c = 0.983$ nm, and $\beta = 94.56°$. It is a new structure of boehmite in comparison to the orthorhombic bulk structure. It involves 3.3 times the lattice volume in an orthorhombic lattice enclosed in a smaller surface area, $S = 3.7 \times 10^3$ m^2/g, as compared to 4.5×10^3 m^2/g in it. This structure forms in a fast Al surface hydrolysis reaction in this example because it undergoes a fast release of its total surface energy as a function of its fast growth. The molecular vibrational structure of AlO(OH)·αH$_2$O nanocrystals is analyzed from their IR spectrum which has three characteristic bandgroups at 200–1200 cm^{-1}, 1300–2500 cm^{-1}, and 2800–4000 cm^{-1}. A considerably improved value of the O–H group stretching frequency by as much as 360 cm^{-1} relative to the bulk value appears for a proton localized structure in the nanocrystals. © 2001 Academic Press

Key Words: X-ray diffraction analysis; IR analysis; AlO(OH)·αH$_2$O nanocrystals; surface hydrolysis of Al metal; monoclinic boehmite crystal structure.

INTRODUCTION

AlO(OH)·αH$_2$O (boehmite) is one of the most important raw materials of aluminum and its oxides. It is the main component of many kinds of bauxites, and regarding the utility of the latter, the structure and properties of the boehmite component play a determining role. Moreover, synthetic boehmite is used in synthesizing electronically

pure transition aluminas or sapphire and Al$_2$O$_3$ composites (1–5). Its microstructure, i.e., particle morphology, size, and separation between particles, plays a major role in monitoring the microstructure and other properties of the product according to experimental conditions. An AlO(OH)·αH$_2$O precursor of confined particle size on a nanometer scale is useful for deriving a nanocrystalline or mesoporous Al$_2$O$_3$ powder by its controlled thermal decomposition at moderate temperature. Today, the two classes of materials are used extensively as heterogeneous catalysts, as absorption media, and in several other optical and electronic devices and components (1–8). Their utility is manifested in their refined microstructures which allow molecules access to large internal surface areas and cavities that enhance catalytic activity and adsorption properties. Mesoporous materials are typically amorphous or nanocrystalline as per their confined dimension of particles and pores on a nanometer scale.

Several methods, e.g., spray pyrolysis (1), gas condensation (2), adiabatic combustion of Al^{3+} salts (3), sol–gel or alkoxide method (4, 9), and surface hydrolysis of Al metal (5), are available for preparing a precursor of AlO(OH)·αH$_2$O. A special advantage of the last method, which is used here, over the other methods is that it easily provides separated AlO(OH)·αH$_2$O particles of a controlled size as small as 20 to 50 nm. They are in a new monoclinic crystal structure in comparison to the D_{2h}^{17} orthorhombic bulk crystal structure (9–12).

In this article, we report a structural analysis of AlO(OH)·αH$_2$O nanocrystals in monoclinic crystal structure using X-ray diffraction and infrared spectrum. The results are discussed in correlation with X-ray diffraction (9–12) and IR or Raman spectroscopy (11–13) of the bulk sample. A confined AlO(OH)·αH$_2$O structure in nanocrystals results in a modified IR spectrum of the bulk sample. It presents a proton localized structure with an improved value of O–H group stretching frequency by as much as 360 cm^{-1} over the bulk value.

[1] To whom correspondence should be addressed. Fax: (091) 3222-55303. E-mail: sram@matsc.iitkgp.ernet.in.

EXPERIMENTAL

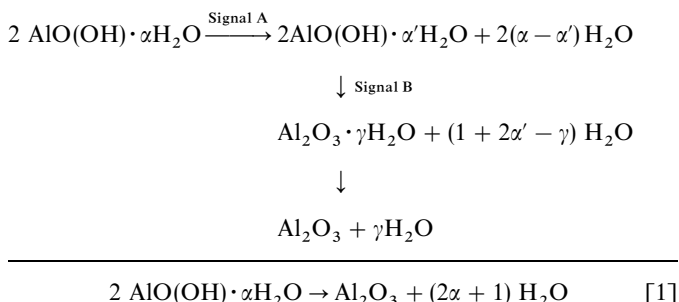### Synthesis

AlO(OH)·αH$_2$O nanocrystals are synthesized by surface hydrolysis of a nascent Al metal in water at room temperature (RT). In this process, flat surfaces of a thin Al metal plate (99.5% pure) of thickness ~ 1.5 mm were degreased, washed in distilled water, and treated with 0.1 M HCl for 10 min. Excess acid, if any, was carefully washed away along with oxidized Al metal at the surface in distilled water. The refreshed Al metal surface still has a thin surface-oxidized layer. As such it does not permit hydrolysis in air or water.

A reactive Al surface is obtained on rubbing the refreshed surface with a small amount (10 mg) of HgCl$_2$. In this process, Hg^{2+} cations, which come in intimate contact with Al metal at the surface, are immediately reduced to Hg metal by an instantaneous coreduction reaction with Al metal through a thinned surface oxide layer, 2Al + 3HgCl$_2$ $\rightarrow$ 2AlCl$_3$ + 3Hg. The obtained Hg metal, in this well-known reaction (5), forms a thin amalgam with the nascent Al surface, and the surface oxides, if any, segregate and float over it. Those are easily washed along with excess HgCl$_2$, if any, and the AlCl$_3$ by-product in distilled water, leaving behind a desirably reactive sample of the nascent Al surface. As soon as it is immersed in distilled water at RT, it rapidly hydrolyzes into AlO(OH)·αH$_2$O nanocrystals with a vigorous exothermic reaction, Al + $(\alpha + 2)$H$_2$O $\rightarrow$ AlO(OH)·αH$_2$O + $\frac{3}{2}$H$_2$. Finally, the AlO(OH)·αH$_2$O sample is filtered and dried at RT. It is a finely divided loose powder. The synthesis of such a refined powder is not so easy by wet methods (1–5), which often result in a wet gel with several by-product impurities.

Measurements and Analysis

The nanocrystalline AlO(OH)·αH$_2$O powder is stable at room temperature. On heating, it desorbs part of the αH$_2$O and dissociates to Al$_2$O$_3$ with two primary thermal signals A and B at ~ 350 and 575 K (5) with 14.0 and 13.1% mass loss, respectively, as follows:

$$2\,\text{AlO(OH)}\cdot\alpha\text{H}_2\text{O} \xrightarrow{\text{Signal A}} 2\text{AlO(OH)}\cdot\alpha'\text{H}_2\text{O} + 2(\alpha - \alpha')\,\text{H}_2\text{O}$$

$$\downarrow \text{Signal B}$$

$$\text{Al}_2\text{O}_3\cdot\gamma\text{H}_2\text{O} + (1 + 2\alpha' - \gamma)\,\text{H}_2\text{O}$$

$$\downarrow$$

$$\text{Al}_2\text{O}_3 + \gamma\text{H}_2\text{O}$$

$$2\,\text{AlO(OH)}\cdot\alpha\text{H}_2\text{O} \rightarrow \text{Al}_2\text{O}_3 + (2\alpha + 1)\,\text{H}_2\text{O} \qquad [1]$$

A trace γ (equivalent to 2.7% mass of the total sample) of H$_2$O remains in the final specimen at 675 K. It is released

monotonically only over higher temperatures to 800 K. A value of $\alpha \approx 0.70$ is calculated from a total of 29.8% loss in mass of the sample in $(2\alpha + 1)$H$_2$O. A reasonably larger $\alpha \geq 1$ appears in the sample derived from sol–gel or other wet methods (5, 9). No Al(OH)$_3$·xH$_2$O forms in this reaction. It has a larger mass loss as small as 34.6% even at $x = 0$. Usually, $x \geq 1$, and it reflects a 47% or larger mass loss.
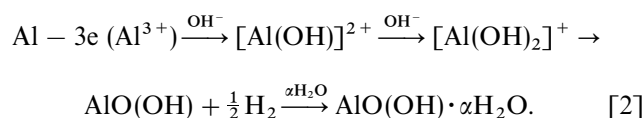
The X-ray diffractogram of the sample is analyzed with a PW 1710 X-ray diffractometer using filtered CoKα radiation of wavelength $\lambda = 0.17902$ nm. The average particle size and microstructural characteristics are studied with a JEM 200CX transmission electron microscope in conjunction with an analyzer for *in situ* studies of electron diffraction. The infrared spectrum (from 200 to 4000 cm^{-1}) is measured for a sample dispersed in a KBr pellet in a 10:90 ratio with a JASCO FTIR-5300 infrared spectrophotometer. The reported frequency values are accurate to ± 2 cm^{-1} for sharp bands and ± 10 cm^{-1} for the broad bands.

RESULTS AND DISCUSSION

Reaction Process

A fast surface hydrolysis of Al atoms occurs at the nascent Al surface in a fast reaction with H$_2$O molecules as soon as the sample is immersed in distilled water at RT. It is a highly exothermic reaction which occurs by chemical dissociation of H$_2$O at the Al metal surface, H$_2$O $\Leftrightarrow$ H$^+$ + OH$^-$. The OH$^-$ anions instantaneously react with Al atoms and hydrolyze them into AlO(OH)·αH$_2$O while the H$^+$ cations are released as H$_2$ gas.

As proposed earlier (5), AlO(OH)·αH$_2$O forms in this example through intermediate reactions in a self-controlled manner in successive steps,

$$\text{Al} - 3\text{e} \,(\text{Al}^{3+}) \xrightarrow{\text{OH}^-} [\text{Al(OH)}]^{2+} \xrightarrow{\text{OH}^-} [\text{Al(OH)}_2]^+ \rightarrow$$

$$\text{AlO(OH)} + \tfrac{1}{2}\text{H}_2 \xrightarrow{\alpha\text{H}_2\text{O}} \text{AlO(OH)}\cdot\alpha\text{H}_2\text{O}. \qquad [2]$$

The metastable [Al(OH)]$^{2+}$ and [Al(OH)$_2$]$^+$ intermediate reaction species appear one after the other. The latter is relatively stabilized and does not react with OH$^-$ anion so rapidly to form a stable Al(OH)$_3$ molecule. As a result, by the time another OH$^-$ group recombines with it and forms a stable product,

$$[\text{Al(OH)}_2]^+ + \text{OH}^- \xrightarrow{x\text{H}_2\text{O}} \text{Al(OH)}_3\cdot x\text{H}_2\text{O}, \qquad [3]$$
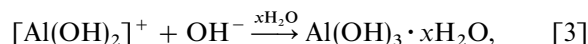
it transforms to an AlO(OH) molecule just by releasing a proton H$^+$. The reaction involves only a minor redistribution of its local properties of internal energy and electronic charges so it occurs fast within a time interval $t_2 \ll t_2'$. Here,

t_2' is the time interval within which the $[Al(OH)_2]^+$ reaction species converts into $Al(OH)_3$ by a recombination reaction with OH^- in Eq. [3] in a confined surface reaction as in this example.

The nascent $AlO(OH)$ molecules arrange in groups in a specific manner according to the experimental conditions. In principle, a group of molecules nucleate and grow into a stable crystal particle if it succeeds in attaining a critical size d^* (diameter). Formation of a surface of stable particles, $d \leq d^*$, of surface area A, adds a surface energy $\Omega = A\sigma$ to the equilibrium Gibb's free energy of the system. In a spherical shaped particle of radius r, it involves a change in the Gibb's free energy,

$$\Delta G = -(\tfrac{4}{3})\pi r^3 \Delta G_v + 4\pi r^2 \sigma, \qquad [4]$$

where σ is the interfacial energy and $\Delta G_v (>0)$ is the change in the Gibb's free energy on its formation from a randomly dispersed assembly of molecules (amorphous structure) (14, 15). It has a maximum $\Delta G^* = 16\pi\sigma^3/3(\Delta G_v)^2$ value at a critical $r = r^* = 2\sigma/\Delta G_v$. Using the numerical $\sigma = 0.70$ J/m^2 and $\Delta G_v = 740$ MJ/m^3 values (15) gives $r^* = 1.9$ nm. It is the minimal r value of the particle which can grow into a stable particle, $r > r^*$. In principle, a structure grows at the expense of its excess Ω energy. A large value of Ω in extremely small particles inputs a retarding potential in the formation of their ordered structure at $\Delta G > 0$. In this case, it is only the volume Gibb's free energy in the first term in Eq. [4] that drives the growth of particle.

Since at $r = r^*$ the sample exists in a nonequilibrium state far above the equilibrium value, the growth of particle occurs very fast to attain a reasonably stable size at $\Delta G \leq 0$.

As per Eq. [4], a value of $r = R \equiv 3\sigma/\Delta G_v$ appears at $\Delta G = 0$. It is 1.5 times larger than the r^* value. Here, we can define the saturation time Δt_s that it takes in growing to R through r^*. The value of Δt_s can be estimated by using the average growth velocity of particle $(r > r^*)$ u with the condition $R = u\Delta t_s$. We studied the equilibrium growth of $AlO(OH)$ in fibers at the nascent Al metal surface in a humid air (16). Fibers as long as 5 mm (30 μm in diameter (16)) grow with an average value of $u = 0.4 \times 10^6$ nm/s within the first 2 min of the reaction. An activated reaction with an order of improved u value occurs in water. Using this average u value together with the numerical value of $R = 1.5r^* \approx 2.9$ nm in the above relation we get a value of $\Delta t_s = 0.7$ μs, which as such is an adequately small value, ascribing a pretty fast chemical reaction to this example. As described elsewhere (14), the value of u and in turn the value of R depends on the driving force of the reaction. This is reasonably large in the $Al - 3e^- \rightarrow Al^{3+}$, with 1.662 V electromotive force (17), surface hydrolysis in this example.

In this fast reaction, $AlO(OH) \cdot \alpha H_2O$ molecules order in a specific crystal structure in a specific morphology of space lattice of average size R to assist the fast release of Ω in the grain growth through R. This is possible with a feasibly large building structure (crystal unit cell) of the particle. This is the case in this example of $AlO(OH) \cdot \alpha H_2O$ in a monoclinic crystal structure which has a lattice volume V that is 3.3 times the orthorhombic bulk structure.

X-Ray Diffraction and Microstructure

The X-ray diffractogram (Fig. 1) of $AlO(OH) \cdot \alpha H_2O$ powder consists of a total of 14 distinct peaks between 10
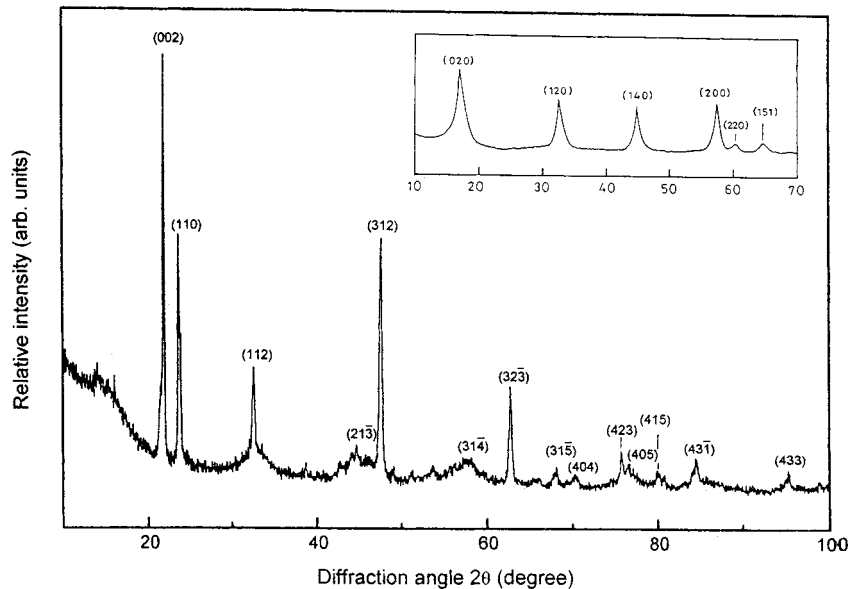

FIG. 1. X-ray diffractogram for $AlO(OH) \cdot \alpha H_2O$ nanocrystals of monoclinic crystal structure (C_{2h}^5 space group). The diffractogram for the bulk crystals is included in the inset.

TABLE 1
Interplanar Spacing d_{hkl} and Relative Intensities (I) of Characteristic Peaks in the X-Ray Powder Diffractogram of AlO(OH)·αH$_2$O Nanocrystals

d_{hkl} (nm)					
Observed	Calculated[a]	I	h	k	l
0.4850	0.4899	100	0	0	2
0.4377	0.4365	59	1	1	0
0.3198	0.3195	29	1	1	2
0.2358	0.2388	12	2	1	$\bar{3}$
0.2210	0.2167	58	3	1	2
0.1872	0.1818	9	3	1	$\bar{4}$
0.1721	0.1681	25	3	2	$\bar{3}$
0.1598	0.1596	4	3	1	$\bar{5}$
0.1560	0.1558	3	4	0	4
0.1458	0.1432	10	4	2	3
0.1430	0.1396	4	4	0	5
0.1392	0.1346	3	4	1	5
0.1332	0.1325	8	4	3	$\bar{1}$
0.1212	0.1210	3	4	3	3

[a] The d_{hkl} values are calculated from the average lattice parameters $a = 0.866$, $b = 0.506$, $c = 0.983$ nm and $\beta = 94.56°$ for the monoclinic crystal structure.

and 100° on the 2θ scale with peak intensity $I \geq 3$. The most intense peak lies at 0.4850 nm with the second and third most intense peaks at 0.4377 and 0.2210 nm, respectively. An analysis of the widths of these peaks by the Debye–Scherrer relation predicts an average crystallite size $d \sim 30$ nm. This diffractogram differs from that in the orthorhombic crystal structure (10). It has a total of 20 different peaks, $I \geq 3$, in this region with lattice parameters $a = 0.370$ nm, $b = 1.222$ nm, and $c = 0.286$ nm (10). For example, part of the diffractogram is included in the inset to Fig. 1. The most intense peak in this case occurs in the (020) reflection at 0.6110 nm with the second and third most intense peaks in the (120) and (140) reflections at 0.3160 and 0.2340 nm, respectively.

All of the peaks observed in this diffractogram are successfully assigned assuming a monoclinic crystal structure (C_{2h}^5 space group) with lattice parameters $a = 0.866$ nm, $b = 0.506$ nm, $c = 0.983$ nm, and angle $\beta = 94.56°$. It has $V = 0.429$ nm^3 and density $\rho = 2.25$ g/cm^3. The most intense peak in this diffractogram is ascribed to the (002) reflection while the second and third most intense peaks are ascribed to the (110) and (312) reflections, respectively. Assignment of the individual peaks along with their relative intensities and (hkl) values is given in Table 1.

The present AlO(OH)·αH$_2$O structure is very similar to the monoclinic structure for Al(OH)$_3$ (5, 18). As compared in Table 2, both structures have $z = 8$ molecules per crystal unit cell in C_{2h}^5 monoclinic crystal structure. Analysis of a monoclinic structure and its lattice parameters from X-ray diffraction pattern is not simple, unlike in other structures. The formulation is scarcely available in the literature. Therefore, we report a complete analysis of it in the following.

In the conventional notation, the position vector of a point P in a crystal plane (hkl) in reciprocal lattice space is written as

$$\mathbf{r}^* = h\mathbf{a}^* + k\mathbf{b}^* + l\mathbf{c}^*, \qquad [5]$$

TABLE 2
Crystal Structure, Lattice Parameters, Density (ρ), Lattice Volume (V), Lattice Surface Area (A), and Lattice Surface Energy (Ω) of Synthetic AlO(OH) and Al(OH)$_3$ Powders

Sample	Nature	Structure/lattice parameters	V (nm^3)	ρ (g/cm^3)[a]	A (10^3 m^2/g)	Ω (kJ/g)
AlO(OH)·αH$_2$O (boehmite)	Porous	Monoclinic $a = 0.866$ nm, $b = 0.506$ nm, $c = 0.983$ nm, $\beta = 94.56°$, $Z = 8$	0.429	2.25 (1.85)	3.7	2.59
AlO(OH) (boehmite)	Bulk	Orthorhombic $a = 0.286$ nm, $b = 1.222$ nm, $c = 0.370$ nm, $Z = 4$	0.129	3.01	4.5	3.15
Al(OH)$_3$ (gibbsite)	Bulk	Monoclinic $a = 0.868$ nm, $b = 0.507$ nm, $c = 0.972$ nm, $\beta = 94.56°$, $Z = 8$	0.426	2.44	3.4	2.38
Al(OH)$_3$ (bayerite)	Bulk	Monoclinic $a = 0.506$ nm, $b = 0.867$ nm, $c = 0.471$ nm, $\beta = 90.26°$, $Z = 8$	0.206	2.53	4.2	2.94

[a] The value of ρ is calculated from the lattice volume. The observed value for porous boehmite is given in parentheses.

where $\mathbf{a}^* = 1/\mathbf{a}$, $\mathbf{b}^* = 1/\mathbf{b}$, and $\mathbf{c}^* = 1/\mathbf{c}$ are the reciprocal lattice vectors. For a monoclinic structure with $\mathbf{a} \neq \mathbf{b} \neq \mathbf{c}$, $\alpha = \gamma = 90°$, and $\beta > 90°$, we can write from Eq. [5],

$$\mathbf{r}^{*2} = h^2 \mathbf{a}^{*2} + k^2 \mathbf{b}^{*2} + l^2 \mathbf{c}^{*2} - 2hl\mathbf{a}^*\mathbf{c}^* \cos \beta, \qquad [6]$$

where $\mathbf{a}^* = (a \sin \beta)^{-1}$, $\mathbf{b}^* = b^{-1}$, and $\mathbf{c}^* = (c \sin \beta)^{-1}$. Using $\mathbf{r}^* = 1/d_{hkl}$ as the interplanar spacing it reduces to

$$\frac{1}{d_{hkl}^2} = \left[\frac{h^2}{a^2} + \frac{l^2}{c^2} - \frac{2hl \cos \beta}{ac} \right] \frac{1}{\sin^2 \beta} + \frac{k^2}{b^2}. \qquad [7]$$

This is the standard working relation, which provides a calculation for the lattice parameters using experimental d_{hkl} values in (hkl) peaks in X-ray diffractogram. It describes the diffractogram of $AlO(OH) \cdot \alpha H_2O$ in Fig. 1 well with a standard deviation of ± 0.005 nm in a, b, and c values.

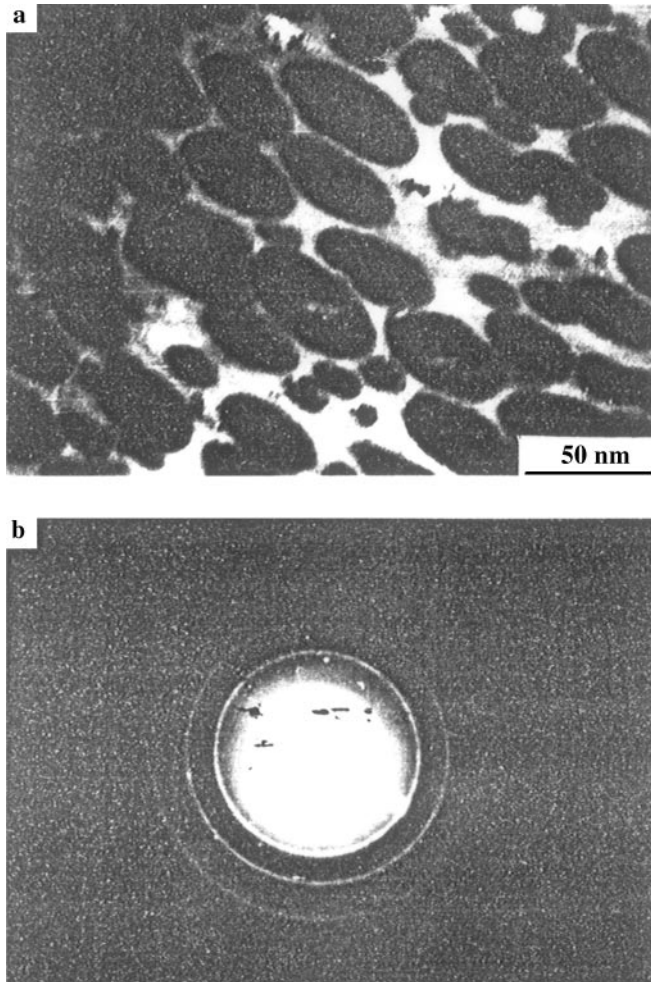**FIG. 2.** (a) TEM micrograph and (b) corresponding electron diffractogram for $AlO(OH) \cdot \alpha H_2O$ nanocrystals.

A TEM micrograph along with the corresponding electron diffractogram for $AlO(OH) \cdot \alpha H_2O$ powder is given in Fig. 2. It shows particles in an ellipsoidal shape of an average $D_{av} \sim 35$ nm diameter and $\varphi \sim 1.8$ aspect ratio. The particles are self-organized in a mesoporous structure through small pores with 2 to 5 nm distance between particles in accordance with the presumably directional Al metal surface hydrolysis. The electron diffraction pattern (Fig. 2b) has four resolved rings at $d_{hkl} = 0.492$, 0.320, 0.237, and 0.190 nm in the (002), (112), (213), and (314) reflections for the monoclinic structure of the sample. These d_{hkl} values compare well with the positions of peaks at 0.4850, 0.3198, 0.2358, and 0.1872 nm in the X-ray diffraction.

The $AlO(OH) \cdot \alpha H_2O$ powder has $\phi = 18\%$ porosity, estimated from the difference in observed density $\rho = 1.85$ g/cm^3 from the theoretical $\rho = 2.25$ g/cm^3 value. As the monoclinic crystal structure involves V as much as 3.3 times that in the orthorhombic bulk structure, it has a smaller A/V ratio, $\cong 8.63 \times 10^{30}$ m^{-1} g^{-1}, over $A/V \cong 34.88 \times 10^{30}$ m^{-1} g^{-1} for the bulk. In a presumably fast reaction, it can be argued that small particles, involving a large Ω value, grow on a building structure which supports a small A/V value. This is achieved if the basic building structure, i.e., the crystal unit cell, starts with a large size as in this example.

Infrared Spectrum

The IR spectrum of $AlO(OH) \cdot \alpha H_2O$ nanocrystals (Fig. 3) has three distinct bandgroups: (i) 200–1200 cm^{-1}, (ii) 2800–4000 cm^{-1}, and (iii) 1300–2500 cm^{-1}. Predominately intense bands in groups (i) and (ii) appear in usual molecular vibrations (cf. Table 3) in $AlO(OH) \cdot \alpha H_2O$ while weak bands in group (iii) arise in a peculiar polymeric structure as discussed below.

Including three OH group fundamental modes (FM) of vibration, i.e. O–H stretching (v), O–H angle bending (β), and O–H deformation (γ), an $AlO(OH)$ molecule, with $N = 4$ atoms, has a total of $3N - 6 = 6$ FM vibrations. Assuming the OH group has a single point mass (X), an $AlO(OH)$ molecule can be described by a simple nonlinear triatomic ($N = 3$) molecule in the C_s the point group. It describes the three skeleton vibrations of (i) X–Al=O symmetric bond stretching (v_1), (ii) X–Al=O asymmetric bond stretching (v_3), and (iii) X–Al=O angle bending (v_2). All of these vibrations are allowed in both IR and Raman spectra in agreement with the observation.

(i) 200–1200 cm^{-1} region. The IR spectrum with an expanded x-scale in order to show a resolved structure of its individual band components is reproduced in Fig. 4. It consists of two triplet bandgroups at 650 and 1050 cm^{-1} with a single sharp band at 365 cm^{-1}. The three components of the 1050 cm^{-1} bandgroup have more or less the
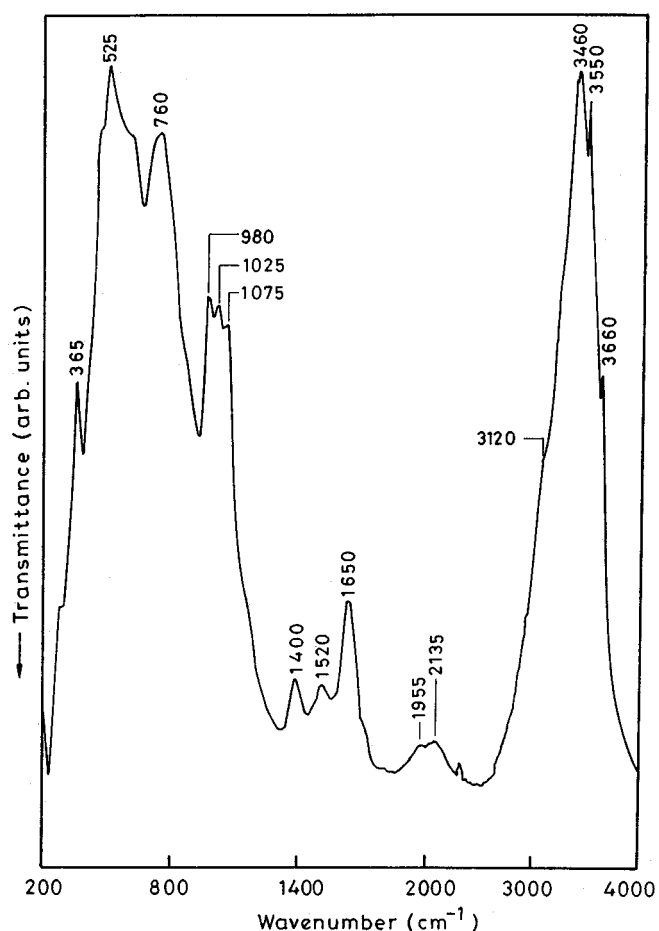
FIG. 3. IR spectrum for $AlO(OH) \cdot \alpha H_2O$ nanocrystals between 200 and 4000 cm^{-1}.

nanocrystals. No such distinct band appears in $AlO(OH) \cdot \alpha H_2O$ bulk crystals (13). It is mixed with the X–Al=O symmetric stretching vibration which is very close in frequency to this band and has the same symmetry. The mixing of the two vibrations is lifted up in a modified O–H force field, evidenced by a considerably enhanced value of the O–H stretching band, as will be discussed in the next section, in a confined nanocrystal. As a result, the vibrations appear in two separate bands. This agrees with the fact that any change in frequency in a bending vibration occurs in a way opposite to that in the stretching vibration (19).

Three components in the 650 cm^{-1} bandgroup lie at 525, 600, and 760 cm^{-1}. The bulk sample has three well-resolved bands at 651, 746, and 770 cm^{-1} (13). On H deuteration, they shift to 677, 555, and 760 cm^{-1} (13). The 525 and 760 cm^{-1} bands involve X–Al=O and Y–O–H angle bending vibrations, respectively, with Y the Al=O group, while the 600 cm^{-1} band represents the O–H deformation vibration. Here, the 525 cm^{-1} band is highly sensitive to local structure because it involves a direct motion of the OH group with respect to the Al=O bond which is relatively rigid in position by its large mass. It has a delocalized character in H-bonding with neighbors and thus it very sensitively influences the frequency in this band. A broad band feature arises in the 600 cm^{-1} band on overlapping with one (rocking) of the three liberation vibrations of H_2O. Another H_2O liberation vibration (wagging) possibly appears in a characteristically sharp band at 365 cm^{-1}. In hydrated salts

same intensity at 980, 1025, and 1075 cm^{-1}. The 980 and 1075 cm^{-1} bands are attributed to X–Al=O symmetric and asymmetric stretching vibrations. Two IR bands occur at 1068 (strong intensity) and 1157 (weak intensity) cm^{-1} in the orthorhombic bulk crystal (13) and at 1022 and 1125 cm^{-1} in amorphous $AlO(OH) \cdot \alpha H_2O$ (16). The Raman spectrum of bulk crystals has a single band at 1053 cm^{-1} (corresponding to the 1068 cm^{-1} band in IR) in this region (13). Unusually, a predominantly large intensity occurs in the IR spectrum for this band (symmetric bond stretching vibration) in bulk crystals, possibly in a proton decollated structure. Otherwise, it would have a smaller intensity than the asymmetric stretching band observed at higher frequency. A proton delocalized structure in $AlO(OH) \cdot \alpha H_2O$ bulk crystals was proposed earlier by Fripiat et al. (11). It modifies the basic intensity distribution in involved vibrations by imposing additional electric dipole moments during the transitions. The effect is predominant in symmetric vibrations.

The remaining 1025 cm^{-1} band in this group is assigned to an in-plane O–H bending vibration in $AlO(OH) \cdot \alpha H_2O$

TABLE 3
Assignments of Vibrational Bands in the IR Spectrum of $AlO(OH) \cdot \alpha H_2O$ Nanocrystals

Frequency (cm^{-1})	Intensity[a]	Assignment
365	ms	H_2O wagging
525	vs	X–Al=O angle bending (v_2)
600	sh	H_2O rocking
760	vs	Y–O–H angle bending
840	sh	H_2O twisting
980	s	X–Al=O symmetric stretching (v_1)
1025	s	O–H bending
1075	ms	X–Al=O asymmetric stretching (v_3)
1400	vw	
1520	vw	Al–O stretching, AlO(OH) dimer
1685	vw	
1650	w	H_2O, v_2 band
1955	vw	$2v_1$
2135	vw	$2v_3$
3120	ms	H_2O, v_1 band
3460	vs	H_2O, v_3 band
3550	vs	O–H stretching
3660	ms	

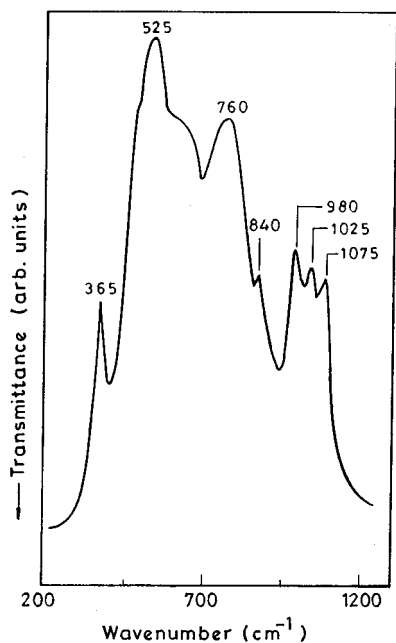[a] vs, very strong; s, strong; ms, medium strong; w, weak; vw, very weak; and sh, shoulder.

FIG. 4. Expanded IR spectrum for AlO(OH)·αH$_2$O nanocrystals on the x-scale in the 200–1200 cm^{-1} region.

(20, 21), three H$_2$O liberation bands lie at 400 to 550 cm^{-1} (wagging), 550 to 750 cm^{-1} (rocking), and ∼850 cm^{-1} (twisting). The H$_2$O twisting vibration in AlO(OH)·αH$_2$O appears as a shoulder of the 760 cm^{-1} band at 840 cm^{-1}.

(ii) 2800–4000 cm^{-1} region. This part of the AlO(OH)·αH$_2$O spectrum describes O–H stretching vibrations in the OH functional group and H$_2$O. As given on an expanded x-scale in Fig. 5, it has resolved components at 3120, 3460, 3550, and 3660 cm^{-1}. The first two bands are broad with bandwidths $\Delta v_{1/2} \sim$ 220 and 280 cm^{-1}, while the others are rather sharp with $\Delta v_{1/2} \sim$ 90 and 80 cm^{-1}, respectively. On the basis of relatively small frequencies and large $\Delta v_{1/2}$ values, the 3120 and 3460 cm^{-1} bands are assigned to v_1 and v_3 vibrations of H$_2$O. In pure ice, the two bands appear at 3150 and 3380 cm^{-1} with a shoulder in a v_2 overtone at 3220 cm^{-1}. They shift to 3450 and 3615 cm^{-1} in liquid H$_2$O and at 3652 and to 3756 cm^{-1} in gas H$_2$O (19). The signature v_2 overtone in the spectrum in Fig. 5 is very much reflected in the asymmetric shape of the 3460 cm^{-1} band at its lower frequency side.

The sharp bands at 3550 and 3660 cm^{-1} represent two localized AlO(OH) molecular vibrations of O–H bond stretching. This is possible if AlO(OH) exists in two conformers with two different orientations of the OH group stabilized by H-bonding. As described by Farmer (22), it forms a layer structure linked by chains of H-bonds through H$_2$O. A reasonably large internal water content, $\alpha \sim 1$, conducts a strong H-bonding, obscuring the resolved features of the two bands. A single unresolved broad ban-

dgroup appears at ∼3400 cm^{-1}, $\Delta v_{1/2} \sim$ 450 cm^{-1}, in a proton delocalized structure (18).

Two O–H stretching bands also occur in bulk AlO(OH) at 3090 and 3297 cm^{-1} (11, 13). They have been interpreted as symmetric and asymmetric stretching vibrations in the O–H group. In principle, a functional OH group as such has a single O–H bond stretching vibration. Moreover, (11), the bands shift to higher frequencies with a progressive decrease in peak intensity on heating the sample at temperature as high as 652 K. They appear at 3215 and 3375 cm^{-1} at 652 K, which are still 285 to 335 cm^{-1} smaller than those in the nanocrystals. This demonstrates that the nanocrystals separated through small pores have a decoupled proton delocalized structure with an enhanced O–H bond strength over the bulk value. A bulk crystal or a strongly H-bonded sample has a proton delocalized structure. In it, discrete vibrational energy levels disappear above a specified level where the probability of the proton tunneling through the potential energy barrier is close to the absorption frequency (11, 13).

(iii) 1300–2500 cm^{-1} region. The IR spectrum in this region (Fig. 3 or 6) has three resolved bands at 1400, 1520, and 1650 cm^{-1} with a shoulder at 1685 cm^{-1}. The 1650 cm^{-1} band, which is the most intense band in this group, is the well-known v_2 band of H$_2$O. The other bands do not occur in bulk AlO(OH)·αH$_2$O in the usual molecular structure. None of them can be interpreted as an overtone or combination band. In this case, it is logical to argue that they arise due to a peculiar amorphous surface structure in
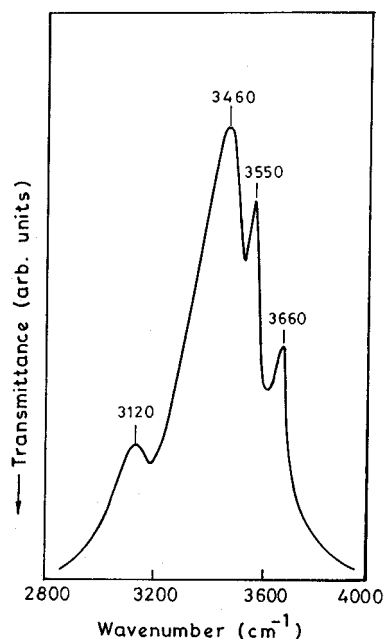

FIG. 5. Expanded IR spectrum for AlO(OH)·αH$_2$O nanocrystals on the x-scale in the 2800–4000 cm^{-1} region.
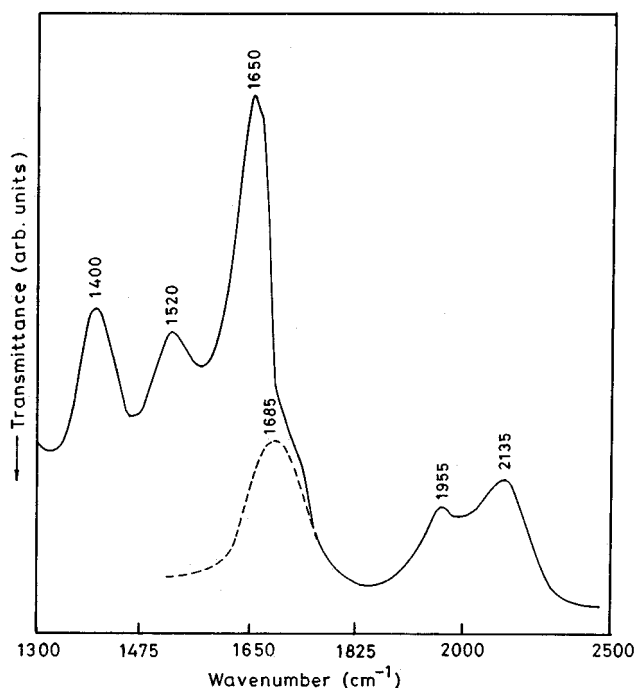
FIG. 6. Expanded IR spectrum for $AlO(OH) \cdot \alpha H_2O$ nanocrystals on the x-scale in the 1300–2500 cm⁻¹ region.

$AlO(OH) \cdot \alpha H_2O$ nanocrystals. The surface layer is stable and this is why the crystalline core remains embedded in its amorphous external shell. The amorphous phase acts as cement to bond nanocrystals which in term form macroscopic particles. The interstices left among the cemented nanocrystals constitute mesopores with active Lewis acid sites exposed inside. The coexistence of crystalline and amorphous components in nanocrystals is consistent with the characteristic diffraction pattern (Fig. 1) with sharp and diffuse lines.

Lewis acid sites in mesoporous solids are of immense interest today owing to their potential applications as surface catalysts, catalyst supports, filler, and other applications (23–25). From CO adsorbed IR studies, Knozinger (23) reported the existence of two kinds of Lewis acid sites in γ-Al_2O_3, which has a similar amorphous surface layer. They originate from uncoordinated tetrahedral and octahedral (or pentahedral) surface Al atoms.

The unsaturated Al^{3+} and O^{2-} ions on the amorphous superficial surface in $AlO(OH) \cdot \alpha H_2O$ nanocrystals rearrange in an interconnected network structure by minimizing the structure's total internal energy. As in conventional vitreous v-B_2O_3 or SiO_2 (26–30), the surface can be generated in a number of ways. In a simple case, it can be described assuming a structural unit of an $AlO(OH)$ dimer as shown in Fig. 7a. Each structural unit can accommodate one H_2O molecule. That lies over its planar structure and stabilizes it by H-bonding through two corner O atoms.

In this model $AlO(OH)$ dimer ring structure, the 1400, 1520, and 1685 cm⁻¹ bands can be ascribed to three Al–O ring stretching vibrations of A, B, and C in Fig. 7 (curves b to d). Displacements of Al and O atoms occur along Al–O–H bonds in vibration A as well as in B. A represents a symmetric vibration while B represents an asymmetric vibration. It is therefore assigned to the 1400 cm⁻¹ band which has a lower value in comparison to 1520 cm⁻¹ in vibration B. In vibration C, the displacements of two Al atoms occur in opposite directions and perpendicular to those in the O atoms along the Al–O–H bond. It therefore refers to the highest frequency band, 1685 cm⁻¹, among these three vibrations. It is also an asymmetric mode of vibration.

This four-membered ring of $AlO(OH)$ dimers can be compared with the six-membered boroxol ring of v-B_2O_3 (26). Both B and Al belong to group IIIB of the periodic table and have the common feature of forming a coordination polyhedron with O^{2-} or OH^- anions. In the boroxol ring, three B–O ring stretching vibrations appear at 1260, 1325, and 1475 cm⁻¹ (26, 28). Their values are very sensitive to the local structure (28). An average 150 to 200 cm⁻¹ larger value in the $AlO(OH)$ dimer is feasible in an Al–O force field marginally larger than that over B–O bonds in boroxol rings.

Another relatively weak bandgroup of two bands occurs in this region (Fig. 5) in $2v_1$ and $2v_3$ overtone bands at 1955 and 2135 cm⁻¹. Assignments of all observed bands in the IR spectrum of $AlO(OH) \cdot \alpha H_2O$ nanocrystals are given in Table 3. A comparison of FM vibrations in crystalline and amorphous samples is made in Table 4.

CONCLUSIONS

$AlO(OH) \cdot \alpha H_2O$ nanocrystals (of an average 35 nm diameter) separated by small pores of 2 to 5 nm diameter are synthesized through a self-induced spontaneous surface hydrolysis of nascent Al metal in pure water at room temperature. Their crystal structure is analyzed by X-ray diffraction. It has a new monoclinic structure with lattice parameters $a = 0.866$ nm, $b = 0.506$ nm, $c = 0.983$ nm, and angle $\beta = 94.56°$ in comparison with the orthorhombic bulk structure. It has 3.3 times the volume of the orthorhombic lattice with surface energy $\Omega = 2.59$ kJ/g (3.15 kJ/g in orthorhombic). $AlO(OH) \cdot \alpha H_2O$ forms in this peculiar structure because the structure facilitates a fast release of structural energy as a function of its fast growth in this reaction. In this condition, $AlO(OH) \cdot \alpha H_2O$ readily attains a thermodynamic equilibrium value of its surface-to-volume ratio.

The IR spectrum of $AlO(OH) \cdot \alpha H_2O$ nanocrystals has three distinct band groups: (i) 200–1200 cm⁻¹, (ii) 2800–4000 cm⁻¹, and (iii) 1300–2500 cm⁻¹. The band positions and relative intensities in these bands are modified significantly in comparison to those in the bulk sample. The bands

HO —— Al
Al —— OH

O O
• Al
● OH

(a)

A
1400 cm⁻¹
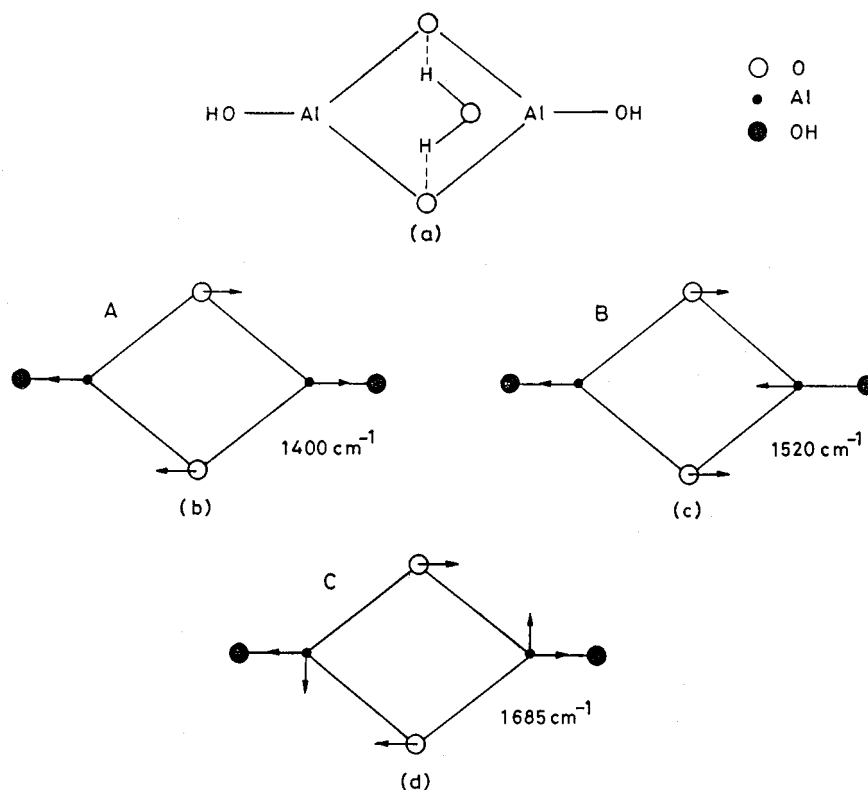(b)

B
1520 cm⁻¹
(c)

C
1685 cm⁻¹
(d)

FIG. 7. Schematic representations of (a) AlO(OH) dimer and (b–d) its A, B, and C three Al–O ring stretching vibrations.

in (i) and (ii) groups are assigned to six AlO(OH) fundamental vibrations and three fundamental and three lattice vibrations of αH_2O. Two O–H stretching vibrations appear in the coexistence of AlO(OH) in two conformers in two different orientations of the OH group stabilized by H-bonding through H_2O. AlO(OH)·αH_2O molecules form a layer structure linked by H-bonds. The bands shift considerably from 3090 and 3297 cm⁻¹ in bulk to 3550 and 3660 cm⁻¹, i.e., by as much as 360 cm⁻¹ in the nanocrystals. This demonstrates a proton localized structure in AlO(OH)· αH_2O nanocrystals. Otherwise, a bulk crystal has a proton delocalized structure in which movement of

TABLE 4

Characteristics IR Bands (in cm⁻¹) for Fundamental Modes of Vibration in Amorphous and Crystalline AlO(OH)·αH_2O Powders

	Amorphous		Crystalline	
	EC method[a]	Gel method[a]	Orthorhombic[b]	Monoclinic
HO–Al=O Group Vibrations				
O–H stretching	3460	3200–3600	3090, 3297	3550, 3660
O–H bending				1025
X–Al=O stretching (v_1)	1022	1070	1068	980
X–Al=O angle bending (v_2)	600	632	651	525
X–Al=O stretching (v_3)	1125	1150	1157	1075
Y–O–H angle bending	600	620	770	760
H₂O Vibrations				
O–H stretching (v_1)				3120
H–O–H angle bending (v_2)	1640	1650		1650
O–H stretching (v_3)				3460

[a] Values are reported from Ref. (16).

[b] Values are reported from Ref. (13).

a proton is extended through the whole structure. In the proton delocalization process (11, 13), discrete vibrational energy levels disappear above a specified level where the probability of proton tunneling through the potential energy barrier is close to the absorption frequency.

The other bandgroup has three distinct components (excluding H_2O bending band at 1650 cm^{-1}) at 1400, 1520, and 1685 cm^{-1}, which are ascribed to three Al–O stretching vibrations in a model ring structure of $AlO(OH) \cdot \alpha H_2O$ dimer. This bandgroup does not appear in the bulk sample. It arises in a peculiar amorphous surface structure in nanocrystals. The amorphous phase behaves as a cement to bond nanocrystals which in turn form macroscopic particles. The interstices left among the cemented nanocrystals constitute mesopores with active Lewis acid sites exposed inside. The coexistence of amorphous and crystalline $AlO(OH) \cdot \alpha H_2O$ components in nanocrystals is consistent with an X-ray diffractogram with sharp and diffuse lines in reflections from different lattice planes.

ACKNOWLEDGMENTS

REFERENCES

1. D. S. Albin and S. H. Risbud, *Adv. Ceram. Mater. A* **23,** 242 (1987).
2. R. W. Siegel, *Annu. Rev. Mater. Sci.* **21,** 559 (1991).
3. V. Hlavacek, *Ceram. Bull.* **70,** 240 (1991).
4. T. Yazawa, K. Kadona, H. Tanaka, T. Sakaguchi, S. Tosubota, K. Kuaoka, M. Mira, and W. D. Xian, *J. Non-Cryst. Solids* **170,** 105 (1994).
5. S. Ram and S. Rana, *Mater. Lett.* **42,** 52 (2000).
6. C. G. Wu and B. Thomas, *Science* **264,** 1758 (1994).
7. H. Yang, N. Coombs, I. Solokov, and G. A. Ozin, *Nature (London)* **381,** 589 (1996).
8. W. Cai, Y. Zhang, J. Jai, and L. Zhang, *Appl. Phys. Lett.* **73,** 2709 (1998).
9. B. E. Yoldas, *in* "Ultra structure processing of advanced ceramics" (J. D. Mackenzie and D. R. Ulrich, Eds.), p. 333. Wiley, New York, 1988.
10. JCPDS file 21.1307.
11. J. J. Fripiat, H. Bosmans, and P. G. Rouxhet, *J. Phys. Chem.* **71,** 1097 (1967).
12. G. Mariotto, E. Cazzanelli, G. Carturan, R. D. Maggio, and P. Scardi, *J. Solid State Chem.* **86,** 263 (1990).
13. A. B. Kiss, G. Keresztury, and L. Farkas, *Spectrochim. Acta A* **36,** 653 (1980).
14. A. B. Pevtsov, V. Y. Davydov, N. A. Feoktistov, and V. G. Karpov, *Phys. Rev. B* **52,** 955 (1995).
15. A. Paul, "Chemistry of glasses." Chapman & Hall, London, 1990.
16. S. Ram, T. B. Singh, and L. C. Pathak, *Phys. Stat. Sol. (a)* **165,** 151 (1998).
17. S. Ram and S. Rana, *Curr. Sci.* **77,** 1530 (1999).
18. JCPDS file 12.460.
19. W. A. Senior and W. K. Thompson, *Nature* **205,** 170 (1965).
20. S. Ram, *J. Raman Spectrosc.* **18,** 537 (1987).
21. V. P. Tayal, B. K. Srivastava, D. P. Khandelwal, and H. D. Bist, *Appl. Spectros. (Rev.)* **16,** 43 (1980).
22. V. C. Farmer, *Spectrochim. Acta A* **36,** 585 (1980).
23. H. Knozinger, *in* "Adsorption on Ordered Surfaces of Ionic Solids and Thin Films" (H.-J. Freund and E. Umbach, Eds.), Springer Series in Surface Sciences 33. Springer-Verlag, Berlin, 1993.
24. V. Gruver and J. J. Fripiat, *J. Phys. Chem.* **98,** 8549 (1994).
25. L. J. Alvarez, L. E. Leon, J. F. Sanz, M. J. Capitan, and J. A. Odriozola, *J. Phys. Chem.* **99,** 17872 (1995).
26. A. K. Hassan, L. M. Torel, L. Borjesson, and H. Doweidar, *Phys. Rev. B* **45,** 12797 (1992).
27. M. Fujii, M. Wada, S. Hayashi, and K. Yamamoto, *Phys. Rev. B* **46,** 15930 (1992).
28. S. Ram, *Phys. Rev. B* **51,** 6280 (1995).
29. H. Z. Zhuang, X. W. Zou, Z. Z. Jin, and D. C. Tian, *Phys. Rev. B* **52,** 829 (1995).
30. S. Ram and K. Ram, *Infrared Phys. Tech.* **37,** 457 (1996).